33rd Annual International Conference of the IEEE EMBS
Boston, Massachusetts USA, August 30 - September 3, 2011

Automated Spatial Alignment of 3D Torso Images

Arijit Bose, Shishir K. Shah, Gregory P. Reece, Melissa A. Crosby, Elisabeth K. Beahm, Michelle C. Fingeret, Mia K. Markey, and Fatima A. Merchant

***Abstract*— This paper describes an algorithm for automated spatial alignment of three-dimensional (3D) surface images in order to achieve a pre-defined orientation. Surface images of the torso are acquired from breast cancer patients undergoing reconstructive surgery to facilitate objective evaluation of breast morphology pre-operatively (for treatment planning) and/or post-operatively (for outcome assessment). Based on the viewing angle of the multiple cameras used for stereophotography, the orientation of the acquired torso in the images may vary from the normal upright position. Consequently, when translating this data into a standard 3D framework for visualization and analysis, the co-ordinate geometry differs from the upright position making robust and standardized comparison of images impractical. Moreover, manual manipulation and navigation of images to the desired upright position is subject to user bias. Automating the process of alignment and orientation removes operator bias and permits robust and repeatable adjustment of surface images to a pre-defined or desired spatial geometry.**

I. INTRODUCTION

BREAST reconstruction is a component of the surgical procedures for some women undergoing breast cancer treatment. Recent advances in imaging technology have made it possible to acquire three-dimensional (3D) images of patients. This has necessitated the development of image analysis methods to provide quantitative information on breast morphology for surgical planning and outcome assessment. For example, quantitative measurements include the use of distances between fiducial points (anatomical landmarks) to define breast appearance in terms of symmetry [1] and ptosis [2]. Automating the computation of distances requires automated identification of fiducial points. The fiducial point localization process relies on the 3D image being orthogonal to the viewing geometry [3], which is often difficult to ensure in practice. Acquisition of 3D data is performed based on the principles of stereophotography [4], and may result in an oblique view of the patient torso [5]. Figure 1A presents an image of the torso acquired using the DSP 800 (3Q Technologies, Atlanta, GA), which depicts the non-upright view of the torso. In addition, the positioning of the patient can vary from one individual to the other, thereby adding to the uncertainty of the image orientation. To overcome this limitation, we propose an automated method for image alignment based on analyzing the underlying mesh geometry of the 3D image. Alignment results from the automated algorithm are evaluated to assess performance and robustness of the method. Inter- and intra-observer variability for the alignment process from several observers is recorded, and the algorithm's performance is compared to that of the manual alignment process.

Manuscript received April 15, 2011. This work was supported in part by NIH Grant 1R01CA143190-01A1 and American Cancer Society grant RSGP-09-157-01-CPPB.

A. Bose is with the Department of Computer Science, University of Houston, Houston, TX 77204 USA (e-mail: jit.bose@gmail.com).

S. K. Shah is with the Department of Computer Science, University of Houston, Houston, TX 77204 USA (e-mail: sshah@central.uh.edu).

G. P. Reece is with the Department of Plastic Surgery, The University of Texas MD Anderson Cancer Center, Houston, TX 77030 USA (e-mail: greece@mdanderson.org).

M. A. Crosby is with the Department of Plastic Surgery, The University of Texas MD Anderson Cancer Center, Houston, TX 77030 USA (e-mail: macrosby@mdanderson.org).

E. K. Beahm is with the Department of Plastic Surgery, The University of Texas M. D. Anderson Cancer Center, Houston, TX 77030 USA (e-mail: ebeahm@mdanderson.org).

M. C. Fingeret is with the Department of Behavioral Science, The University of Texas MD Anderson Cancer Center, Houston, TX 77030 USA (e-mail: mcfinger@mdanderson.org).

M. K. Markey is with the Department of Biomedical Engineering, The University of Texas at Austin, Austin, TX 78712 USA (e-mail: mia.markey@mail.utexas.edu).

F. A. Merchant is with the Department of Engineering Technology, University of Houston, Houston, TX 77204 USA (phone: 713-743-8292; fax: 713-743-0172; e-mail: fmerchant@uh.edu).

The authors recognize the support and contributions of any patient data that were generously provided by Geoff Rodd, M.D. and Steven Kronowitz, M.D., the Department of Plastic Surgery at MD Anderson Cancer Center for use in this study.

II. SPATIAL ALIGNMENT OF 3D SURFACE IMAGES

The objective of this study is to develop an algorithm for the automatic alignment of 3D torso images to the upright forward facing position. This orientation allows uniform quantitative assessments to be performed and facilitates the implementation of algorithms for localization of fiducial points, which rely on a forward facing and upright orientation of the torso [6]. Moreover, automation facilitates robust and speedy processing, supports batch processing of multiple images, and eliminates operator bias.

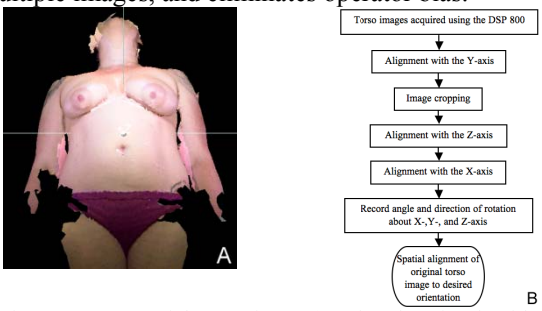

Fig. 1. (A) Non-upright torso image (B) Flowchart for algorithm.

The flowchart in Figure 1B outlines the algorithm for automatic spatial alignment of 3D surface images to a pre-defined or desired spatial geometry.

A. *Upright Alignment of the 3D surface along the Y-axis*

The orientation of surface geometry is defined by the direction of the normal vector [7]. Following acquisition of the 3D torso image, we compute the surface normal for each triangle of the surface mesh as follows. For each triangular face of the mesh, if a and b are the two vectors denoting the two sides, then the normal vector is defined as $normal = a \times b$. The surface normal of the 3D surface (n) is then computed as $n = \frac{(normal * \Delta)}{\Delta}$, where Δ is the area of each triangular face in a mesh. The 3D torso is then aligned orthogonal to the X-axis in order to achieve an initial forward facing upright orientation. The angle of rotation about the X-axis is determined as:

$$\alpha = \tan^{-1}\left(n_y / n_z\right) \quad \text{and} \quad \begin{bmatrix} 1 & 0 & 0 \\ 0 & \cos\alpha & -\sin\alpha \\ 0 & \sin\alpha & \cos\alpha \end{bmatrix} \qquad (1)$$

where n_y and n_z represent the y, and z components of the surface normal, and the transformation matrix defines the rotation of the 3D surface by α about the X-axis [7].

B. *Image cropping*

In order to further fine-tune this initial alignment, the torso data are cropped to remove the arms and neck regions of the torso. This was implemented because the area of the arms, neck and legs captured in the 3D image is influenced by the width and height of the subject, respectively. This results in variability in the extent of the surface captured and image asymmetry. Thus, in order to achieve symmetrical uniformity, the neck, arms and legs of the torso image were cropped as follows. First, the 3D points are projected on the YZ plane. Figure 2A shows the histogram for the 3D torso points projected on the YZ plane. The valleys in the plot denote the location along the Y-axis where the image can be cropped to remove the neck and legs from the torso. These points are automatically computed by computing the slope dz/dy of the histogram.

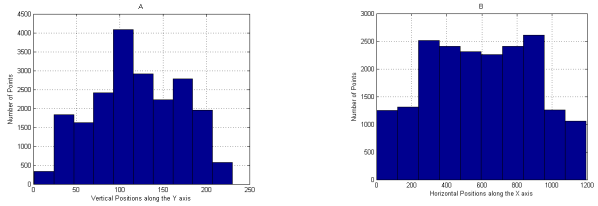

Fig. 2: (A) Histogram of 3D torso points projected on the YZ plane, (B) Histogram of 3D torso points projected on the XY plane that exhibits maximal information in the Z-direction.

For example, the y coordinate, with the steepest decrease in the slope is noted as the cutoff crop point for the neck, beyond which the image needs to be cropped. Similarly, to crop the arms, multiple XY projections of the torso are obtained along the Z-axis. The XY projection exhibiting the maximum count of y points for each corresponding x point is selected, and the slope dy/dx of the corresponding histogram (see Figure 2B) is computed.

Then traversing to the right of the centroid (center of mass of 3D point cloud) along the X-axis, the x coordinate exhibiting the maximum slope (steepest descent) denotes the location where the right arm should to be cropped. Similarly, traversing from the centroid to the left of the torso, we find the corresponding location at which the left arm should be cropped. Figure 3A shows the torso subsequent to the cropping of the arms, legs, and neck portions of the torso.

Fig 3: (A) The 3D torso subsequent to image cropping for neck/legs and arms, (B) Final upright forward facing 3D torso obtained from automated alignment.

C. *Forward facing alignment of the 3D surface along the Z-axis*

The 3D torso is then aligned along the Z-axis to orient it in the forward facing direction. First, the surface normal of the cropped and smoothed 3D surface is computed as defined in equation (1). If n_x; the x component of the surface normal is negative, the torso faces towards the left, and if n_x is positive the torso faces toward the right. In order to obtain a forward facing orientation, the angle of rotation about the Y-axis is determined as:

$$\beta = \tan^{-1}\left(n_x / n_z\right) \quad \text{and} \quad \begin{bmatrix} \cos\beta & 0 & -\sin\beta \\ 0 & 1 & 0 \\ \sin\beta & 0 & \cos\beta \end{bmatrix} \qquad (2)$$

is the transformation matrix to rotate the 3D surface by β about the Y-axis [7].

D. *Horizontal alignment of the 3D surface along the X-axis*

Finally, the 3D surface is aligned horizontally along the X-axis to orient the shoulders straight laterally. The surface normal of the torso after rotation about the Y-axis is computed. The angle of rotation about the Z-axis is determined as:

$$\gamma = \sin^{-1}\left(n_x / \sqrt{\left(n_x^2 + n_y^2\right)}\right) \quad \text{and} \quad \begin{bmatrix} \cos\gamma & -\sin\gamma & 0 \\ \sin\gamma & \cos\gamma & 0 \\ 0 & 0 & 1 \end{bmatrix} \qquad (3)$$

is the transformation matrix to rotate the 3D surface by γ about the Z-axis [7].

E. *Final Alignment of the torso*

The angles of rotation α, β, and γ about the Y-, X-, and Z-axes, respectively, determined above are used to obtain the final alignment of the raw data (unprocessed data acquired from the DSP 800). The final orientation of the torso is shown in Figure 3B.

III. Methods and Materials

A. Imaging System

The 3D surface images were obtained using the DSP 800 (3Q Tech., Atlanta, GA). Each reconstructed surface image consists of 3D positions (*x*, *y*, *z*) and their corresponding color and texture information.

B. Study Population

Four Female patients (both breasts and nipples intact) who were scheduled for breast reconstruction surgery at The University of Texas MD Anderson Cancer Center were recruited for this study under a protocol approved by the institutional review board (IRB). In addition, four healthy female volunteers were commissioned under contract to participate in the study. The subjects (patients and volunteers) ranged in age from 30 to 64; 7 were white, 1 was african american.

C. Study Design & Data Analysis

Three observers manually aligned 3D images of the subjects using customized software developed by our group [5]. Two trials of alignments were performed at an interval of two weeks to include analyses of intra- and inter-observer variability. An upright forward facing manual alignment of the eight surfaces performed by an independent observer was chosen as the gold standard. Surfaces aligned using manual and automated methods were compared using the relative angle context distribution (RACD) signature described next.

D. Relative Angle Context Distribution (RACD)

Relative Angle Context Distribution (RACD) establishes the 3D point correspondence around a vertex in a surface mesh with all the other vertices with respect to the relative reference frame calculated using principal component analysis (PCA) [8]. The probability mass function of the resulting relative angle distribution defines the RACD; which can be used to determine the point correspondence between two 3D surfaces. The similarity between a pair of 3D surface images can then be determined by comparing the distributions of the global relative angles context for corresponding points on the two surfaces. In this study in order to expedite processing, five points were used as the corresponding points at which the similarity between two surfaces was computed: centroid (center of mass), left nipple, right nipple, umbilicus, and sternal notch. First, the dissimilarity (d_k) between the RACD of two corresponding points of the manually aligned, or automatically aligned 3D surfaces with the gold standard was computed as follows [8]

$$d_k\left(v_i, v'_j\right) = \left\| p_k(v_i) - p'_k\left(v'_j\right) \right\| \quad (5)$$

where $v_i \in V$ (set of 5 points including the centroid, left and right nipple, sternal notch and umbilicus) of surface (manually aligned or automatically aligned), and $v'_j \in V'$ set of 5 points including the centroid, left and right nipple, sternal notch and umbilicus) of surface (gold standard), and $p_k(v_i)$ and $p'_k\left(v'_j\right)$ are the probability mass functions. The similarity factor (*sf*) between the two 3D surfaces was computed as follows [8]

$$sf = \sum_{i=1}^{N} \left(1 - d_k\left(v_i, v'_i\right)\right) \Big/ N \quad (6)$$

where v and v' represent the corresponding points in the two surfaces being compared and N is the total number of points. This method of comparing two 3D surfaces was validated using a symmetric 3D conical model surface as shown in Figure 4A.

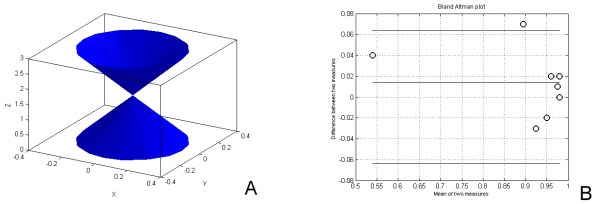

Fig. 4: (A) 3D conical model used to validate the use of the RACD signature to compare two 3D surfaces, (B) Bland-Altman Plot comparing the *sf* of automated alignments with manual alignments.

The model surface was independently rotated by 30° about the X-axis, and each rotated model was compared to original model to compute the similarity between the two surfaces using the RACD method and similarity factor. Following validation, the similarity factor was applied to compare the results of automated alignment with that of manual alignment.

E. Statistical Analysis

Intraclass Correlation Coefficient (ICC) was used for assessing the consistency or reproducibility of quantitative measurements made on the same subject. ICC<0.4 indicates poor reproducibility, 0.4≤ICC<0.75 indicates fair to good reproducibility, and ICC≥0.75 indicates excellent reproducibility [9]. ICC was used to determine the inter- and intra-observer variability in the manual alignment of 3D surfaces based on the similarity factor measurements. A Bland-Altman plot, which provides a visual and qualitative assessment of the agreement between two methods, was used to compare the similarity factor from manual alignment to that from the automated alignment [10].

IV. Results

A. Measurement of similarity between two 3D surfaces

The RACD signature was first validated as an indicator of similarity between two 3D surfaces. The similarity factors determined using the RACD signature for comparing the model following defined rotations about the X-axis to the original model (unrotated, i.e., 0°) are shown in Table 1. A similarity factor of 1 indicates the same surface, whereas 0 indicates dissimilarity between the two surfaces being compared. As seen in Table I, the *sf* is 1 when comparing the original model (0°) to itself. Following rotations, the similarity between the rotated surface and the original surface decreases and increases back to 0.99 (~1) for the 180° rotation. These comparisons validate the use of the RACD signature for comparing two 3D surfaces.

TABLE I

VALIDATION OF THE RACD SIGNATURE AS A SIMILARITY INDEX FOR COMPARING 3D SURFACES

Rotation about the X-axis (°)	Similarity Factor (*sf*)
0	1.00
30	0.88
60	0.75
90	0.22
120	0.15
150	0.33
180	0.99

B. Inter- and Intra-observer variability

Manual alignment of the 3D torso by three different observers was assessed by comparing the manually aligned surfaces with the gold standard. The following assessments were performed (1) comparison of alignments performed by the same observer at two time points (two weeks apart), and (2) comparison of alignments performed by the two different observers. ICC was used to determine the consistency of manual alignments. There was excellent agreement in the spatial alignment performed in the two trials by all three observers. The ICC values for alignments made in trial1 and trial2 by observer1, observer2, and observer3 were found to be 0.78, 0.95, and 0.98 respectively. Table II presents data on the inter-observer variability. Overall, there was excellent agreement in the spatial alignment performed by different observers, with the exception of only a moderate agreement between Observer1 and Observer3 in trial 1.

TABLE II
ICC VALUES FOR INTER-OBSERVER MEASUREMENTS

		ICC
Trial 1	Obs 1 – Obs 2	0.80
	Obs 2 – Obs 3	0.96
	Obs 1 – Obs 3	0.64
Trial 2	Obs 1 – Obs 2	0.97
	Obs 2 – Obs 3	0.94
	Obs 1 – Obs 3	0.95

C. Performance evaluation of automated spatial alignment

Finally, the automatically aligned surfaces were compared with the gold standard. The similarity factors obtained by comparing the manually aligned surface from trial 1, and the automatically aligned surfaces with the gold standard for the 8 subjects are shown in Table III.

TABLE III
SIMILARITY FACTOR FOR MANUAL (TRIAL1) & AUTOMATED ALIGNMENTS

Subject	*sf*			
	Observer1	Observer2	Observer3	Automated
1	0.60	0.88	0.99	0.93
2	0.99	0.97	0.98	0.97
3	0.97	0.99	1.00	0.98
4	1.00	0.97	0.98	0.96
5	0.91	0.91	0.91	0.91
6	0.58	0.50	0.51	0.56
7	0.94	0.99	0.94	0.94
8	0.94	0.99	0.94	0.98

The manual spatial alignments taken over the two trial sessions by the three observers were averaged to obtain the reference set and used to assess the automated spatial alignment algorithm developed. The percentage of the difference between the two measurements divided by the mean of the two sets of measurements was computed as the relative error of magnitude (REM) [11]. REM scores less than 1% are deemed "excellent;" between 1 and 3.9%, "very good;" between 4 and 6.9%, "good," between 7 and 9.9%, "moderate" and finally anything above 10%, "poor" [11]. The REM score for the automated alignment algorithm was found to be 2.8%. Finally, a Bland-Altman plot was used to compare the automatic spatial alignment's similarity factor with that of the reference set. As seen from Figure 4B, the similarity factor in the spatial alignment made by the reference set (average value of all observers over all trials) and the algorithm are within 1.96 times the standard deviation bounds.

V. DISCUSSION

We present an algorithm for the automated spatial alignment of 3D torso images to the forward facing upright and straight position. Automating the process of alignment and orientation removes operator bias and permits robust and repeatable adjustment of surface images to a pre-defined or desired spatial geometry. The algorithm performs with a precision level of "precise" with a REM score of 2.8% (very good). The realignment allows uniform quantitative assessments to be performed and facilitates automated detection of fiducial points [6]. Future work, will compare the proposed method with existing 3D object alignment approaches, and evaluate the efficacy of automated fiducial point detection on the realigned images.

REFERENCES

[1] A. Losken, I. Fishman, D. Denson, H. Moyer, and G. Carlson, "An Objective Evaluation of Breast Symmetry and Shape Differences Using 3-Dimensional Images," Ann Plast Surg, vol. 55, no. 6, pp. 571-575, 2005.

[2] M. S. Kim, G.P. Reece, E.K. Beahm, M.J. Miller, E.N. Atkinson, M. K. Markey, "Objective assessment of aesthetic outcomes of breast cancer treatment: measuring ptosis from clinical photographs," Computers in Biology and Medicine, vol. 37, no. 1, pp. 49-59, 2007.

[3] M. Dabeer, et al. "Toward decision support for breast reconstruction: automated calculation of symmetry measure on clinical photographs," in *Proc* AMIA Annu Symp Proc, vol. 1045, November 2008.

[4] D.B. Sheffer, et al. "Stereophotogrammetric method for breast cancer detection," Proceedings of the SPIE - The International Society for Optical Engineering, vol. 361, pp. 120-124, 1982.

[5] J. Lee, et al. "Validation of Stereophotogrammetry of the Human Torso," Breast Cancer: Basic and Clinical Research, vol. 5, pp. 515-525, 2011.

[6] M. Kawale, "Automated Identification of Fiducial Points on Three-Dimensional Torso Images," M.S. thesis, Dept. Comp. Sc., University of Houston, Houston, TX, 2010.

[7] J.X. Chen, E. J. Wegman, "Foundations of 3D graphics programming: using JOGL and Java3D," London: Springer, 2006.

[8] J. Feng, H.S. Ip. Horace, L.Y. Lai, A. Linney "Robust point correspondence matching and similarity measuring for 3D models by relative angle-context distributions," Image and Vision Computing, vol. 26, pp. 761–775, 2008.

[9] K. O. McGraw, S. P. Wong, "Forming inferences about some intraclass correlation coefficients," Psychological Methods, vol. 1, pp. 30-46, 1996.

[10] J. M. Bland, D. G. Altman, "Statistical methods for assessing agreement between two methods of clinical measurement," Lancet, vol. 327, no. 8476, pp. 307-310, 1986.

[11] T. E. Mutsvangwa, J Smit, H. E. Hoyme, W. Kalberg, D. L. Viljoen, E. M. Meintjes, and S. T. Douglas," Design, Construction, and Testing of a Stereo-Photogrammetric Tool for the Diagnosis of Fetal Alcohol Syndrome in Infants," IEEE Trans. Medical Imaging, vol. 28, no. 9, September 2009.